Analysis and Design Improvement of a Spacecraft Thermal Deflector

Pedro Francisco de Matos Diogo Baião Abraços
pedro.abracos@tecnico.ulisboa.pt

Instituto Superior Técnico, Lisboa, Portugal

November 2015

Abstract

This thesis is focused on the development of methodologies to perform structural and thermal finite element analyses to characterise the behaviour of spacecraft cork-agglomerate-based sandwich thermal deflectors with composite facesheets, using commercial finite element analysis software. To do this, experimental tests were conducted on specimens to perform the characterisation of the materials involved, focusing on the storage modulus and the damping factors associated with both the CFRP facesheets and cork core. Static properties were determined using a three-point bending test for the sandwich specimen. For the dynamic properties, the RFP algorithm was used on the modal analysis response spectrum for modal parameters' identification. A model updating procedure was then applied to the FEM to obtain the adjusted constitutive models. To verify the operational characteristics of the deflector, a thermal finite element analysis was implemented for a radiation/conduction coupled problem, using a view-factor method in grey-diffuse bodies. Analytical verifications were performed to the FEM. Parametric studies were then used to determine design changes that would lead to a reduction in the heat radiated towards the satellite. A final solution is proposed for the thermal design of the deflector: apply MLI on the surface facing the satellite and a reflective white paint coating on the one the nozzle. The thermal requirements were then all met and the maximum temperature in the deflector is below that of the maximum working temperature of the cork agglomerate ($180^{\circ}C$). It was concluded that this design presented better thermal insulation than typical titanium deflectors.

Keywords: Spacecraft thermal deflector, Finite element model, Cork agglomerate, View factor method, Thermal analysis

1. Introduction

The aerospace industry is in constant demand for lightweight, high strength and reliable components. Nowadays, there are already investigations taking place to introduce new materials into the aeronautical industry, namely cork composites, that fulfil these requirements [4].

These materials have, however, low resilience, which could be mitigated by introducing viscoelastic materials in the equation which act as a good vibration and impact attenuator, as well as a thermal insulator. As such, cork could prove to be a viable option to improve the thermal (e.g., low conductivity associated with cork) and mechanical performances of carbon fibre reinforced composites.

Cork agglomerates have been used in space mostly in ablative thermal protection systems (TPS) for re-entry and for solid rocket boosters [4]. Composites are already being used as structural components, mainly truss members, solar array structures and antenna booms [13].

Thermal deflectors are often used in geostationary satellites' apogee boosters, which are turned on to both correct and change orbital parameters, but primarily to transfer a satellite from the geostationary transfer orbit to the geostationary orbit itself. These deflectors are usually conical and assembled as exemplified in Figure 1.

The design of a thermal deflector that uses cork as a non-ablative means of protecting a satellite from the radiation emitted from his engine avoids the usage of titanium-based deflectors, which have a large density and are hard to manufacture [11].

Papers published in this area are scarce, according to the author's research. The most relevant preliminary studies regarding the structural behaviour of composite thermal deflectors, for space applications,

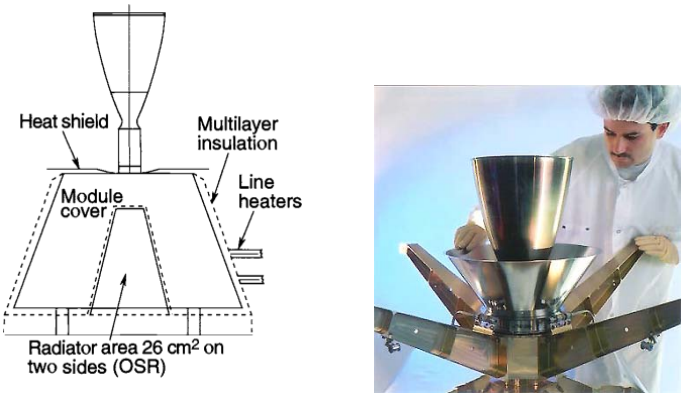

(a) (b)

Figure 1: Examples of thermal deflectors and their location. a) Schematic view of a thermal deflector mounted on a satellite [10]; b) Heat shield mounted below an apogee motor exit nozzle [7].

have been conducted by Barros [5], while Ricardo [4] has studied the application of cork composites in aeronautics.

Due to the lack of readily available information, the work developed aims to create an analysis methodology to determine if a sandwich composite thermal deflector with a cork agglomerate core is able to successfully withstand the thermal and mechanical boundary conditions imposed during operation. These analyses are conducted using a commercial finite element software (in this case, ANSYS® Workbench) and the procedure is verified using experimental tests, analytical calculations performed using MATLAB® and Microsoft® Excel™ routines.

The present document is organised in five main parts: the first section provides a brief description of the viscoelastic behaviour of materials and principles of radiation heat transfer; the second section focuses on the specimens' fabrication procedures, their finite element model, experimental structural tests conducted to characterise the materials and constitutive models' adjustment via model updating (using FEMTools®); the third part deals with the FEM of the deflector itself and the thermal analyses performed using a radiation view factor method; finally, conclusions regarding the applicability of the proposed methodology are issued and possible improvements to be performed in future work addressed.

2. Background

2.1. Viscoelastic Materials

The behaviour of a material when subjected to dynamic or static loads depends on the physical and geometrical properties of that same material. The three main categories of materials according to their stress-strain curve behaviour are elastic, viscoelastic and plastic.

Viscoelastic materials, such as cork agglomerates, exhibit properties that are a combination of the ones enumerated above. Stress application lags in phase behind strain, with the strain being time-dependant (see Figure 2a and 2b). Viscoelasticity works as a damping phenomenon (viscoelastic damping) and, thus, is inherently only dynamically observable.

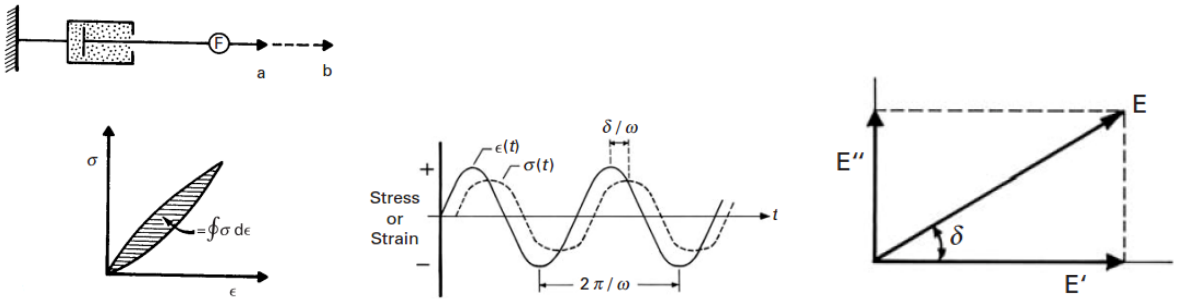

(a) (b) (c)

Figure 2: Equivalent model and stress-strain curve for and viscoelastic materials [9]. a) Viscoelasticity model; b) Stress/strain vs. time curve; c) Storage and complex moduli.

This phase difference and dependence of the elasticity (E), shear (G) and bulk (K) moduli as well as damping properties (described by the loss factor $\eta = \tan\delta = E''/E'$) on frequency can be accounted for by introducing the concepts of storage and complex moduli, shown in Figure 2c. These can be mathematically described by:

$$E^* = E(1 + i\eta) = E' + iE'' \tag{1}$$

It is assumed that the loss factor is the same for all variables (E, G, K and η). Another way to relate these quantities is by using the following definition:

$$E^* = \frac{\sigma(t)}{\epsilon(t)} e^{i\delta} \rightarrow \begin{cases} E' = \frac{\sigma_0}{\epsilon_0}\cos(\delta) \\ E'' = \frac{\sigma_0}{\epsilon_0}\sin(\delta) \end{cases} \tag{2}$$

with σ_0 and ϵ_0 being the amplitude of both stress and strain.

Linear viscoelasticity can be considered for small displacements and it is valid if the final configuration of a body can be determined by linear combination of several load substeps. Since we are working with small displacements, this assumption is used throughout the present work.

2.2. Material Properties

The determination of the storage modulus of viscoelastic materials, such as the cork agglomerate used in the deflector, can be performed using several techniques. One of these techniques is proposed by Policarpo et al [1], described with detail in his thesis [12]. In this method, a two material bar is used (see Figure 3) to solve an inverse characterisation problem using modal experimental techniques.

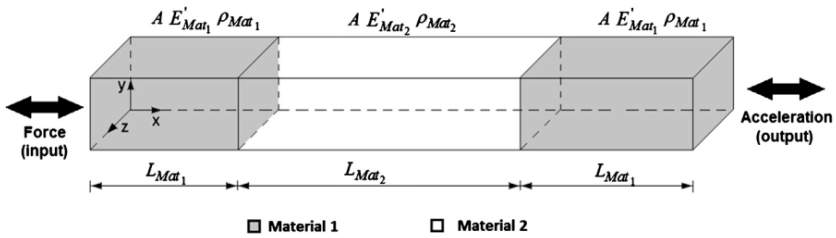

Figure 3: Three layer, two material bar subjected to forced excitation on one end with the resulting acceleration measured on the other end [1].

The material of interest (material 2, with unknown properties) is placed between two blocks of identical dimensions and material properties which are known. The cross-sectional area A is uniform throughout the bar and the materials are characterised by their density ρ and storage modulus E'. This method can also be used to determine the loss factor η of the material of interest and, consequentially, the dynamic modulus E''.

A simple approach can be obtained considering that the mass of material 2 (M_{Mat_2}), which is measured in an adequate device, is much smaller than M_{Mat_1} (mass of the blocks in the extremities of the beam) and that these last bodies are rigid, this system can be represented by a discrete two degree-of-freedom model where the middle body is considered to be a massless spring. Simplifying the system as having 2 degrees-of-freedom, the first natural frequency of the model is [1]:

$$\omega_1 = \sqrt{\frac{2k_{Mat_2}}{M_{Mat_1}}} \Leftrightarrow 2\pi f_1 = \sqrt{\frac{2E'_2 A_2/L_2}{\rho_1 A_1 L_1}} \Rightarrow E'_2 = 2\pi^2 f_1^2 \rho_1 L_1 L_2 \tag{3}$$

where $f_1 = \omega_1/(2\pi)$, $M_{Mat_1} = \rho_{Mat_1} A_{Mat_1} L_{Mat_1}$ and $k_{Mat_2} = E'_{Mat_2} A_{Mat_2}/L_{Mat_2}$ and $A_1 = A_2$ because the cross-section has a constant area. As mentioned in Policarpo et al [1], this model is simplistic and lacks some accuracy, but for these materials if it offers somewhat good results. However, this method is very fast and simple to apply in a laboratorial context.

2.3. Heat Transfer Fundamentals

One of the goals of this study is, as it was previously mentioned, to conduct a thermal analysis on the deflector model to perform a design verification and improvement.

In orbit, the main heat transfer phenomena for solid bodies are radiation and conduction (because there is almost a perfect vacuum in space, no convection occurs outside a spacecraft).

The mechanisms associated with the radiative heat transfer phenomenon to and from a surface can be represented with the schematic in Figure 4a. The radiation that reaches a surface is called the *irradiation* G. Because real bodies do not absorb all incident radiation, a part is reflected (called *reflection* G_{ref}), another part is absorbed and another part is transmitted if the body is not completely opaque. The sum of the portion that is reflected (ρ), transmitted (τ) and absorbed (α) must be equal to 1. The energy that is emitted from the surface (E) summed to the energy that is reflected results on the *radiosity* J of that surface:

$$J(\lambda, T) = E + G_{ref} = \epsilon(\lambda, T)\sigma T^4 + \rho(\lambda, T)G \tag{4}$$

(a) (b)

Figure 4: Radiation model and view factor definition. a) Radiation exchange to and from a surface [8]; b) View factor between elemental surfaces dA_i and dA_j [8].

The view factor F_{ij} corresponds to the fraction of radiation, between 0 and 1, that reaches a surface j coming from surface i. The generic expression for the view factor between two surfaces can be derived from the radiation exchange between two differential areas, dA_i and dA_j. Considering the differential element from Figure 4b and integrating, the overall view factor from surface i to j can be calculated using the following relation [8]:

$$F_{ij} = \frac{1}{A_i}\int_{A_i}\int_{A_j}\frac{\cos(\theta_i)\cos(\theta_j)}{\pi R_{ij}^2}dA_i dA_j \tag{5}$$

with θ_i being the angle between the area normal and the lines that connects the centroids of the areas involved and R_{ij} is the length of that line (distance between the surfaces). If $\theta_i = \theta_j = 0°$ (the area normals are aligned and facing each other), then $F_{ij} = A_j/(\pi R_{ij}^2)$.

The heat flow q_i $[W]$ emitted by surface i to other N surfaces can be calculated by using the following equation [8]:

$$q_i = \sum_{j=1}^{N}\frac{J_i - J_j}{1/(A_i F_{ij})} \tag{6}$$

It must be noted that planar surfaces do not "see" themselves, which means that no heat flow is radiated from a point in the surface to another point belonging to the same planar surface. In these cases, $i \neq j$. For three-dimensional surfaces, this restriction does not apply (the interior of a cone, for example, can radiate heat between two points on the same surface).

The view factor can be computationally determined by using Nusselt's hemicube method, which can be consulted in the full thesis document.

Besides the view factor, there is a quantity called Gebhart's Factor, B_{ij}, which derives from the definition of the former and expresses the fraction of energy absorbed by a particular body when compared to the total radiation emitted by another body. This factor can be estimated by using equation 7 for an enclosure with N surfaces:

$$B_{12} = F_{12}\epsilon_2 + \sum_{k=1}^{N}\left[(1-\epsilon_k)F_{1k}B_{k2}\right] \ , \ k = 1, 2, ..., N \tag{7}$$

It is hard to determine this factor because its calculation depends on the value of the Gebhart factor for another surface (B_{12} depends on B_{k2}, for example). As such, this value has to be determined iteratively.

3. Structural Analysis Methodology

The geometry of the deflector to be considered for the analysis is the following:

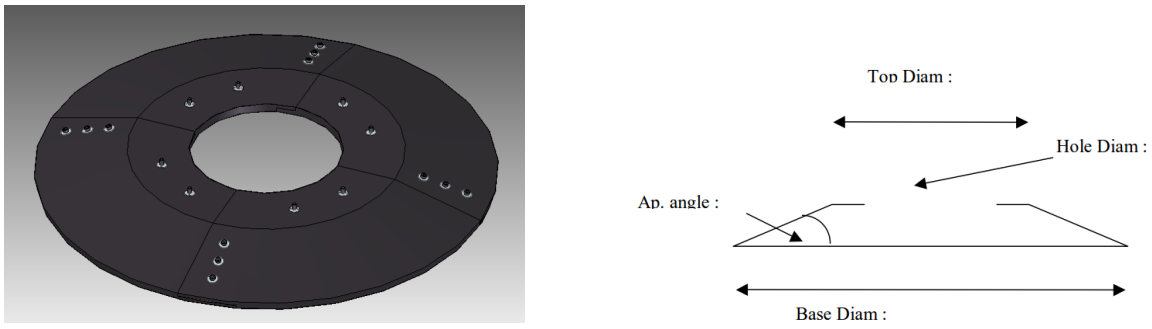

(a) CAD drawing. (b) Overall dimensions schematic.

Figure 5: Geometry of the thermal deflector.

The deflector is composed of 4 identical cyclically symmetrical parts. In these, there is a planar surface in which interface inserts between the deflector and the satellite are placed. A conical section is also visible where the screws used to fixate each quarter are placed.

The material properties associated with the laminate constituents (in this case, a cork agglomerate and a carbon fibre and epoxy resin composite) have a certain degree of uncertainty that needs to be investigated. To perform a model updating of the FE model, experimental modal tests were performed on representative specimens, which were built by the author. Three specimens were built: one composed of the laminated bar with a cork agglomerate core to determine the core's storage modulus; one composed of the facesheet's CFRP,; one of the full representative sandwich used in the deflector.

After producing the specimens, experimental modal analysis procedures were used to extract the FRFs of these specimens and, by post-processing, the relevant modal parameters (damping and natural frequencies) necessary to perform the model updating process. The test schematic is presented in Figure 6. These procedures were first validated by performing the analysis on a steel plate of known properties.

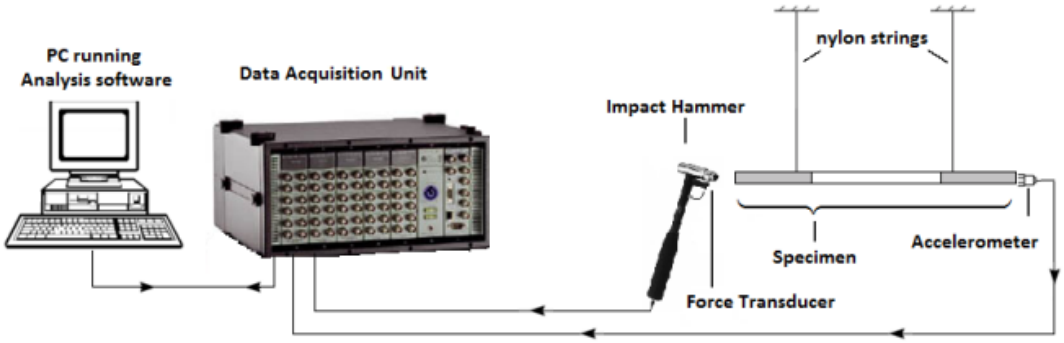

Figure 6: Setup schematic for the bar test (used with permission from Policarpo [12]).

3.1. Results and Discussion

For the experimental tests, three types of specimens were built: a CFRP specimen to test the facesheet; a sandwich specimen with cork agglomerate core; the specimen to perform the bar test mentioned before to determine the storage modulus of the cork agglomerate.

Regarding the experimental tests, a representative results' set is presented here for the sandwich bar, after being analysed in MATLAB®, with the code provided by Policarpo [1].

Using the methodology proposed by Policarpo [1], it was possible to determine that the storage modulus of the cork agglomerate was $E'_{cork} \approx 25.656\ MPa$.

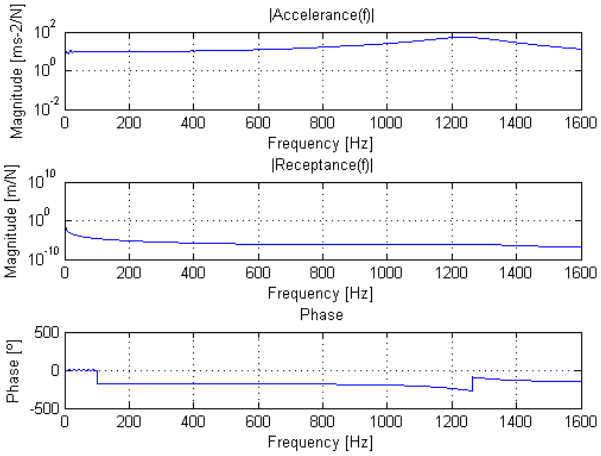

(a)

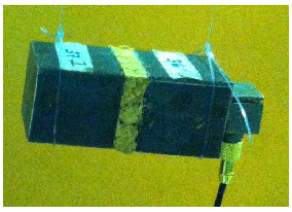

f_1 [Hz]	1248.5
η	0.174
E'_{cork} [MPa]	25.656

(b)

Figure 7: Results of the experimental test for the sandwich bar specimen. a) FRF and mode identification; b) Parameters calculated.

The results for the remaining specimens did not coincide with the results from the FEM analysis. By importing the results to FEMTools®, the model updating software, no converged solution was obtained for the orthotropic/composite specimens (only for the steel plate). This revelaed limitations of the software concerning the model updating of non-isotropic and homogeneous materials.

4. Thermal Analysis

The cork agglomerates used in this work have a maximum operating temperature of about $180°C$ before suffering from mechanical and chemical properties' alterations due to pyrolysis and other effects (as well as the resin used). As such, a thermal analysis needs to be performed to assess the ability of the deflector to withstand operating conditions, both with the engine continuously operating (steady-state) or just operating for a fixed amount of time (transient analysis for an operating time of 300 s).

When an apogee booster is working on a satellite, the following heat transfer boundary conditions can be considered: eadiation exchange between the nozzle and the upper surface of the deflector; radiation exchange $\dot{q}_{rad}$ between the surface of the deflector facing the nozzle and deep-space (a blackbody at 3K); radiation $\dot{q}_{rad}$ from the surface of the deflector facing the satellite and the satellite itself; heat flux from the Sun $\dot{q}_{sun}$, with an intensity of 1367 W/m^2 [10], impinging the surface of the deflector facing the exhaust nozzle; conduction heat flux $\dot{q}_{cond}$ through the interface inserts between the deflector and the satellite.

These boundary conditions are represented in Figure 8's schematic.

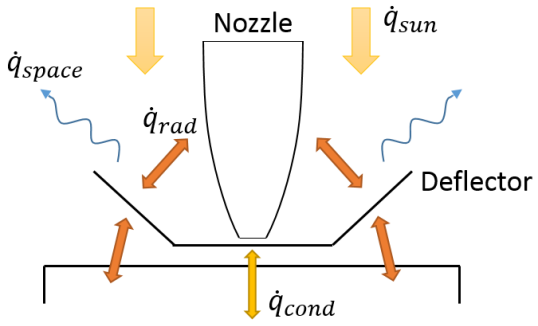

Figure 8: Schematic of the boundary conditions applied to the deflector with the engine operating.

To determine the initial conditions of the deflector with the engine off, no heat flux from the engine to the deflector was considered.

The optical and thermal properties of the materials involved are shown in Table 1.

Material	k $[W/m^2]$	C_p [J/(kg K)]	α	ϵ	ρ $[kg/m^3]$
Carbon fibre	10(x,y), 0.6(z)	710	0.8	0.7	1741.8
Inserts	961.2	-	-	2700	
Nozzle	-	-	-	0.68	8190
Cork Agglomerate	0.036	1975	-	-	250

Table 1: Thermal material properties.

Some cells are filled with "-" because those particular properties were not necessary to completely describe the respective material in the finite element model.

With this information in mind, the methodology from Figure 9 was proposed to conduct the steady-state and transient thermal analyses.

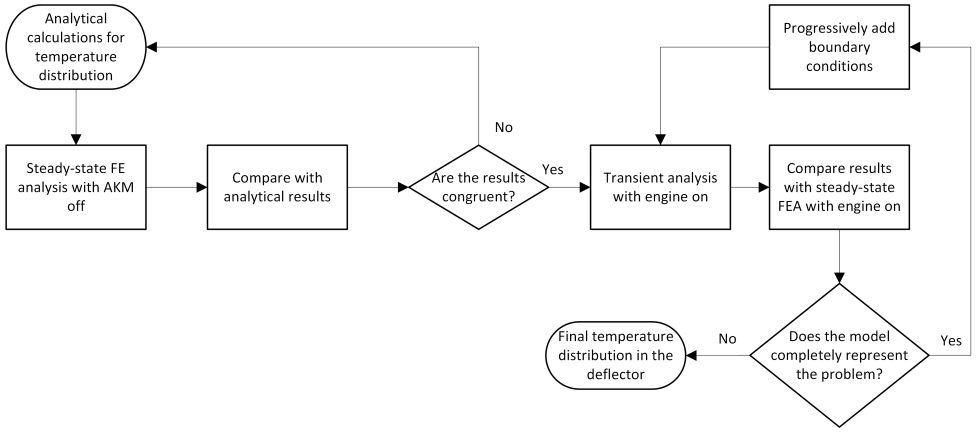

Figure 9: Flowchart of the proposed approach for the thermal analysis of the deflector.

4.1. Analytical Models

As a validation step, the initial temperature T_i of the deflector, approximating it by a circular disk with negligible thickness (uniform temperature), can be calculated using the following expression:

$$T_i = \sqrt[4]{\frac{\alpha}{\epsilon}\frac{q_s(F_s + aF_p)}{B_s\sigma} + \frac{F_p}{B_s}T_p^4 + T_{sur}^4 + \frac{Q}{\epsilon A B_s \sigma}} \tag{8}$$

Without considering the application of thermal coating, considering the deep-space temperature to be $3K$ and the view factor to planet Earth negligible, $T \approx 419.5K$. Details regarding specification of view factors and the deduction of the formula itself can be found in the full thesis document.

The heat flux between the engine and the deflector can also be estimated by using the electrical analogue and considering that the deflector, the engine and deep-space form a three-surface enclosure, as depicted in Figure 10. Moreover, it is considered that all surfaces act as grey bodies, with $\epsilon(\lambda, T) = \alpha(\lambda, T)$. This allows the usage of the radiation network approach method [8], considering that the deflector can be modelled as a circle and the nozzle as a cone.

Deep-space is idealised as a blackbody, which means that $J_3 = E_{b_3} = \sigma T_3^4$. The heat exchange between the engine (1) and the thermal deflector (2) can thus be calculated by using system of equations 9.

$$\begin{cases} \frac{\sigma T_1^4 - J_1}{(1-\epsilon_1)/(\epsilon_1 A_1)} = \frac{J_1 - J_2}{1/(A_1 F_{12})} + \frac{J_1 - \sigma T_3^4}{1/(A_1 F_{13})} \\ \\ \frac{\sigma T_2^4 - J_2}{(1-\epsilon_2)/(\epsilon_2 A_2)} + \frac{q_S}{1/(A_2 F_S)} = \frac{J_2 - J_1}{1/(A_1 F_{12})} + \frac{J_2 - \sigma T_3^4}{1/(A_2 F_{23})} \\ \\ J_1 = \epsilon_1 \sigma \left[F_{12}\left(T_1^4 - T_2^4\right) + F_{13}\left(T_1^4 - T_3^4\right)\right] \end{cases} \tag{9}$$

It is then considered that the nozzle temperature T_1 is fixed and equal to the spatially averaged value of the temperature distribution in that component and the remaining variables can be calculated in order to validate the numerical results.

(a) (b)

Figure 10: Radiation model and definitions used for the analytical calculations. a) Electrical analogue; b) Disk-to-cone view factor schematic [2].

4.2. Numerical Models

The finite element model made use of elements with the same principles as the ones used for the structural analysis, but adjusted for their thermal counterpart. As such, quadratic interpolation elements were also used: SOLID90 for the core and SHELL132 for the facesheets. Several types of contact formulations were tested for application between the facesheets and the core and the *pure penalty* type presented the best results.

Since this problem reveals cyclic symmetry, only a quarter of the deflector needs to be modelled (this is the minimum, since the influence of the fixation inserts between quarters of the deflector needs to be accounted for), greatly reducing simulation times (see Figure 11).

For the case without inserts, the mesh could be created using regular quadrilateral elements. When the inserts were considered, wedge elements had to be used to correctly discretise the geometry. A comparative study was performed between the mesh types and convergence studies performed to ensure that both lead to mathematically correct results.

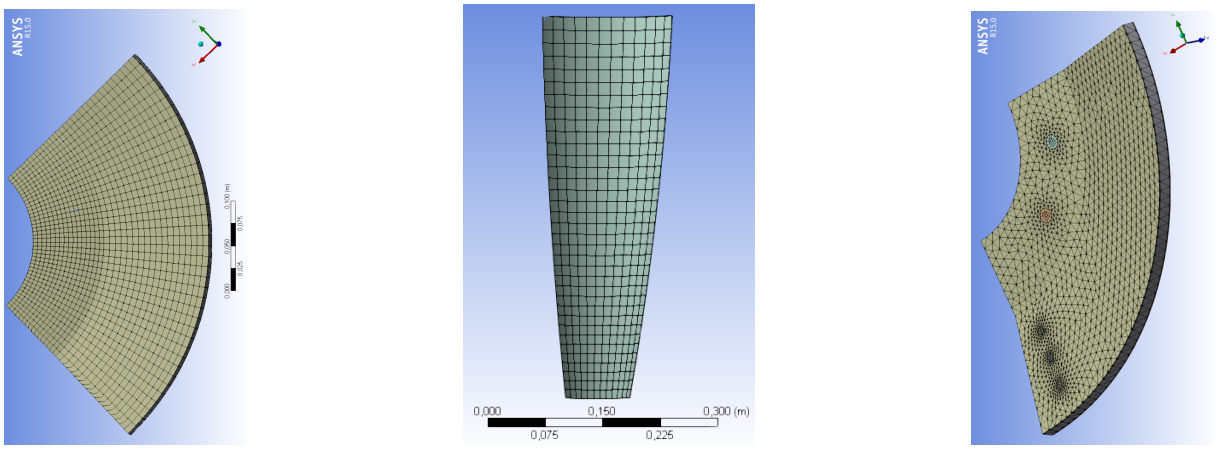

(a) Deflector hex mesh. (b) Nozzle mesh. (c) Deflector wedge mesh.

Figure 11: Finite element meshes for the nozzle and the deflector assembly.

Convergence analyses were also performed for the hemicube resolution, the method used to determine view factors between finite elements in ANSYS® which influence the regularity of the axisymmetric temperature distribution.

4.3. Results and Discussion

For the thermal analysis, the optical parameters of Table 2 were determined for the deflector and surrounding environment.

where α is the absorptivity of the CFRP, ϵ its emissivity, q_p the heat flow coming from planet Earth,

Parameter	Value
α	0.7
ϵ	0.8
q_{sun} $[W/m^2]$	1367
q_p $[W/m^2]$	500
F_s	0.5
F_{sur}	0.5
F_p	0.01
a	0.33
Q $[W]$	7
A $[m^2]$	0.309

Table 2: Optical and radiation parameters used for the thermal analyses.

F_s and F_{sur} are the view factors between the deflector and the Sun and deep-space, respectively, a is the albedo, A is the area of the exhaust nozzle as calculated by ANSYS® Workbench after creating the nozzle's CAD model and Q is the maximum heat dissipation rate for the propulsion module of a Spacebus 4000 satellite. To see the source of these values, please consult the full thesis document.

Initial conditions of the deflector as determined by ANSYS®, using the methodology described above, can be compared with the analytical models presented. This is shown in Table 3, where $T_{max_{initial}}$ refers to the maximum temperature in the deflector with the engine off and the remaining variables are related with conditions with the engine already operating.

Sol. Method	$T_{max_{initial}}$ $[K]$	$T_{max_{final}}$ $[K]$	Q_{engine} $[W]$	$J_{deflector}$ $[W]$
FEM				
Analytical				
Rel. Difference (%)	2.3	4.23	18.85	1.46

Table 3: Comparison between the numerical and analytical thermal analysis' results.

It can be observed that the relative difference in the results is small for the temperature in the case in which the engine is not working and for the energy that is emitted from the deflector, but it becomes large in the other cases, which reveals the limitations on view factor and temperature calculation, which are better described in the thesis. It also reveals that the simplified model to determine view factors led to good results, with a relative difference of just 4.23% when compared to the FE solution.

To ensure that the maximum temperature in the cork core would not be higher than the maximum operating temperature, both a thermal white paint coating (acts as a reflective surface) and multi-layer insulation (MLI) to avoid transferring large amounts of heat towards the satellite were applied to the structure. The design of the MLI was performed by the author and it can be consulted in the full thesis document.

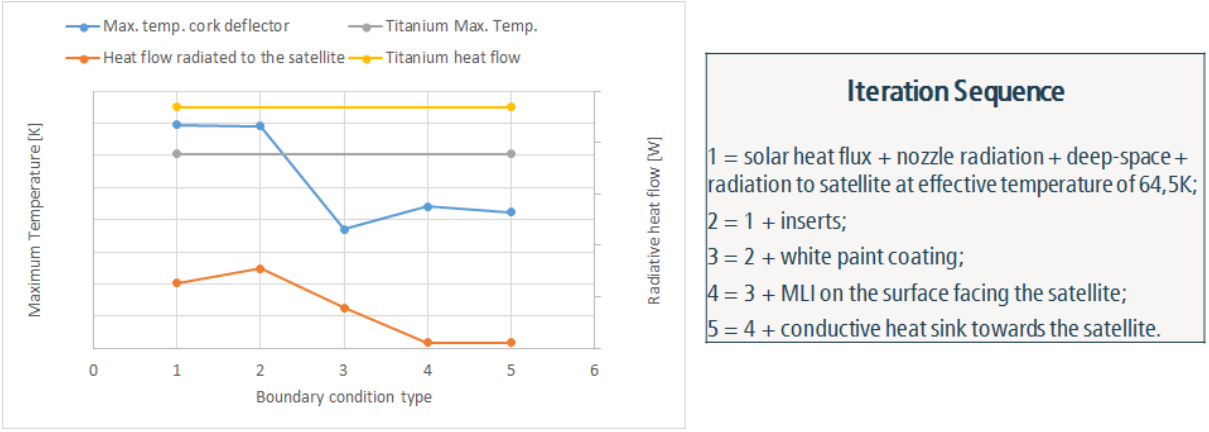

Figure 12: Maximum temperature evolution with boundary condition application.

The sequential application of boundary conditions led to the maximum temperature values in the cork agglomerate core of the deflector shown in Figure 12. In this graph, the radiative heat flow exchanged between the deflector and the satellite is also shown. For comparison purposes, the maximum temperature attained by a titanium thermal deflector without any type of coating and the corresponding radiative heat flow towards the satellite is shown. It can be concluded that the cork deflector radiates a much lower heat flow, even for uncoated conditions, when compared to a titanium deflector. The lower manufacturing and launch costs are complemented by the superior thermal performance of the new cork-agglomerate deflector design.

The final maximum temperature in the cork was found to be lower than the maximum operating temperature fixed for the model, which was of $180°C$. The most significant impact was that of the white paint thermal coating, which acted as a radiation shield due to its very low absorptivity and high emissivity. The final temperature distribution in the cork core in shown in Figure 13.

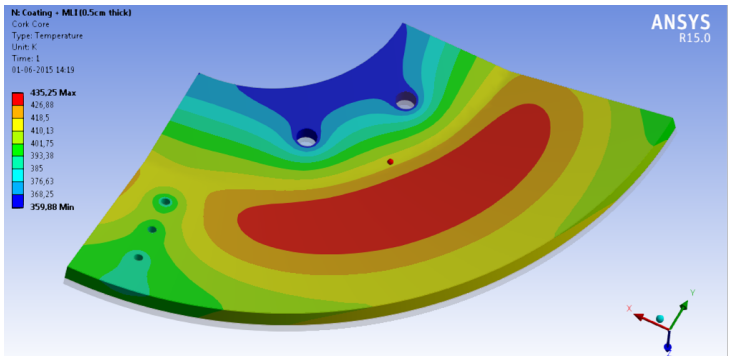

Figure 13: Final temperature distribution in the cork core.

After designing the MLI, parametric studies were performed on selected design variables. To reduce the heat flow towards the satellite and the temperature of the deflector, both the cork thickness t_c and the angle β are likely to have in impact. As such, these will be the design variables.

The corresponding dimensions were parametrised in the *Design of Experiments* module of the FE software. Constraints were applied to the variables: $t_{min} < t_c < t_{max}$ m and $\beta_{min} < \beta < \beta_{max}$.

It was concluded that an optimum design, in a thermal perspective, would be the one with a larger core thickness and also a larger angle in the conical section, since both work towards diminishing the radiative heat flow. However, care must be taken towards the maximum temperature of the core, which must not overcome 453 K. This design optimisation process would need to be further studied but, for the time frame of this thesis, this step could not be completed.

5. Conclusions

It was concluded that laminated thermal deflectors based on CFRP and cork agglomerates offer a viable alternative to the usual titanium designs, from the point of view of their thermal performance, even if the design may not present a large advantage in terms of launch mass. The fact that the laminated deflector radiates less towards the satellite means that the on-board radiators and cooling systems will not have to dissipate as much heat, lowering costs. However, the strict maximum temperatures allowed for this type of deflector means that it is mandatory to use optical coatings like white paints which will also add a penalty to the launch mass and, if they are damaged, the efficiency of the deflector is jeopardised.

A good characterisation of the thermal behaviour of the deflector can be performed using commercial finite element analysis software like ANSYS®. This program has several limitations, namely the fact that it does not work with non-grey-diffuse bodies, which introduces modelling errors. This issue can be mitigated by introducing a "ficticious" dissipative heat flow that mimics the difference between absorptivity and emissivity.

In future works, static, harmonic and transient thermal-structural analyses need to be performed on the deflector to analyse if the temperature gradients in the deflector may jeopardise its structural integrity. The thermal behaviour of the deflector should also be experimentally determined by using thermal-vacuum tests. The properties of the cork agglomerate should also be experimentally assessed in terms if directional variability and the Poisson coefficient should be directly or indirectly determined using other than the assumption of isotropy. The deflector should also be analysed for extreme operation capabilities, namely in the case a portion of optical coating is removed due to an in-flight collision.

References

[1] H. Policarpo et al On a hybrid analytical experimental technique to assess the storage modulus of resilient materials using symbolic computation. Journal of Symbolic Computation, num. 61-62, pp. 31-52, 2014.

[2] Naraghi et al. Radiation configuration between disks and a class of axisymmetric bodies. Journal of Heat Transfer, vol.104, num. 3, pp. 426-431, August 1984.

[3] Airbus. A350xwb: Intelligent and aerodynamic airframe. website, accessed on the 5th of March 2015. http://www.a350xwb.com/advanced/fuselage/.

[4] João Daniel Ramos Ricardo. Structural modelling validation of cork composites for aeronautical applications. Master's thesis, Técnico Lisboa, 2009.

[5] Tiago Barros. Preliminary structural analysis of a thermal deflector of carbon fiber and cork sandwich for space applications. Master's thesis, Técnico Lisboa, 2014.

[6] Boeing. 787 dreamliner: Program fact sheet. website, accessed on the 5th of March 2015. http://www.boeing.com/boeing/commercial/787family/programfacts.page.

[7] Airbus Defence and Space. 400 n bipropellant apogee motors. website, accessed on the 15th of March 2015. http://cs.astrium.eads.net/sp/spacecraft-propulsion/apogee-motors/.

[8] Frank P. Incropera et al. *Introduction to Heat Transfer*,John Wiley and Sons, Inc., 2011.

[9] John D. Ferry. *Viscoelastic Properties of Polymers*. Wiley, 1980.

[10] David G. Gilmore. *Spacecraft Thermal Control Handbook, Volume I: Fundamental Technologies*. The Aerospace Press, 2002.

[11] Kennametal. Titanium machining guide. Technical Document, accessed on the 6th of August 2015. https://www.kennametal.com/content/dam/kennametal/kennametal/common/Resources/Catalogs-Literature/Industry

[12] Hugo Policarpo. *Numerical and Experimental Models for Vibration Attenuation using Cork Composite Materials*. PhD thesis, Técnico Lisboa, 2013.

[13] Thomas P. Sarafin, editor. *Spacecraft Structures and Mechanisms - From Concept to Launch*. Microcosm, Inc and Kluwer Academic Publishers, 4th edition, 2003.

[14] Jos M. Silva et al. Cork: Is it a good material for aerospace structures? In *52nd AIAA/ASME/ASCE/AHS/ASC Structures, Structural Dynamics and Materials Conference*, number 2011-2159. AIAA, April 2011.